Materials and Design 51 (2013) 466–473

Contents lists available at SciVerse ScienceDirect

Materials and Design

journal homepage: www.elsevier.com/locate/matdes

Microstructural evolution and mechanical properties of dissimilar Al–Cu joints produced by friction stir welding

C.W. Tan [a,b], Z.G. Jiang [a], L.Q. Li [a,*], Y.B. Chen [a], X.Y. Chen [a]

[a] State Key Laboratory of Advanced Welding and Joining, School of Materials Science and Engineering, Harbin Institute of Technology, Harbin 150001, China
[b] Center for Advanced Materials Joining, Department of Mechanical and Mechatronics Engineering, University of Waterloo, Waterloo, Canada N2L 3G1

ARTICLE INFO

Article history:
Received 6 March 2013
Accepted 14 April 2013
Available online 24 April 2013

Keywords:
Non-ferrous metals and alloys
Friction stir welding
Intermetallic compounds
Microstructure
Mechanical properties

ABSTRACT

5A02 aluminum alloy and pure copper were joined by friction stir welding (FSW). A defect-free joint was obtained when one of process parameters, i.e. the traverse speed was lowered from 40 mm/min to 20 mm/min. A good mixing of Al and Cu was observed in the weld nugget zone (WNZ). A large amount of fine Cu particles were dispersed in the upper part of the WNZ producing a composite-like structure. In the lower part, nano-scaled intercalations were observed and identified by transmission electron microscopy (TEM). These layered structures were subsequently confirmed as Al_4Cu_9 (γ), Al_2Cu_3 (ε), Al_2Cu (θ), respectively. Formation of these microstructures caused an inhomogeneous hardness profile. Particularly, a distinct rise in hardness was noticed at the Al/Cu interface. Excellent metallurgical bonding between Al and Cu gave rise to good behaviors in the tensile and bending strength.

1. Introduction

Products made of dissimilar material combinations have been becoming increasingly significant in industrial applications because of their technical and economic benefits [1–3]. Aluminum (Al) and copper (Cu) are two common engineering materials widely used in the aerospace, transportation and electric power industries. Al/Cu bimetallic dissimilar joint, is of great interest in electrical connections since it can reduce materials costs and weight while prolonging the service life [4–6]. Welding technique has been considered as a top priority for fabricating this dissimilar joint. Sound joining technique is indispensable for obtaining reliable Al/Cu joint. Conventional fusion welding is, however, not applicable for joining Al to Cu due to their huge differences in physical and chemical properties [7,8]. Moreover, easy formation of cracking and brittle intermetallic compounds (IMCs) is expected in fusion welded joint because of high affinity between Al and Cu, which seriously deteriorates the mechanical properties. Therefore, many kinds of welding techniques such as cold roll welding [9,10], diffusion bonding [11,12], explosive welding [13,14] and friction welding [15–18] have been developed as alternative joining processes for joining Al to Cu. However, disadvantages of the aforementioned processes such as large limitations in joint design, the need to maintain welding condition and cost of procedure have restricted their application in industry.

Friction stir welding (FSW) is a relatively novel solid-state technique patented by the welding institute (TWI) in 1991 [19]. Compared with conventional fusion welding processes, it shows many advantages such as high quality and flexibility. Additionally, FSW has great potential for joining dissimilar materials such as Al to Cu since it allows dissimilar combination under the condition of a lower temperature and a lower heat input. It could mix them together without any melting, which eliminates many defects existed in the fusion welding. Therefore, many recent studies have investigated dissimilar joining Al to Cu by FSW. To the best of our current knowledge, Murr et al. [20] first reported sound welds without any defect were difficult to obtain using FSW. Afterwards, Ouyang et al. [21] investigated the microstructural evolution during FSW of Al to Cu and concluded complex microstructure with several IMCs such as Al_2Cu, AlCu and Al_4Cu_9 was observed. In addition, they claimed that direct FSW of Al to Cu was difficult due to the brittle nature of IMCs. Abdollah-Zadeh et al. [22,23], however, studied the feasibility of FSW of Al and Cu in lap configuration rather than butt configuration. Similar to the aforementioned studies, IMCs such as Al_2Cu, AlCu and Al_4Cu_9 were also observed. Xue et al. [24,25] studied the effect of process parameters such as tool offsetting, rotation rate and traverse speed on microstructure and mechanical properties of dissimilar 1060 aluminum-pure copper joints. They reported defect-free joints with good mechanical properties were achieved, which was attributed to excellent metallurgical bonding caused by formation of thin IMC layer and IMC particles. That was to say, IMCs was not necessarily detrimental to the mechanical strength provided the thickness was controlled to micro scale. Similar phenomenon was observed by Galvão et al. [26–30], Liu et al. [31] and Genevois et al. [32].

The previous studies have mainly addressed the microstructure and mechanical properties of Al–Cu dissimilar joint. Nevertheless,

* Corresponding author. Tel./fax: +86 451 86415506.
E-mail addresses: liliqun@hit.edu.cn, liliqun116@gmail.com (L.Q. Li).

0261-3069/$ - see front matter © 2013 Elsevier Ltd. All rights reserved.
http://dx.doi.org/10.1016/j.matdes.2013.04.056

limited literature has focused on the formation mechanism of the microstructure. In particular, the relationship between microstructure and mechanical properties has not been well established. The objective of the present study is, therefore, to focus on the microstructure and their formation mechanism. The relationship between microstructure and mechanical properties is investigated as well.

2. Experimental details

The materials used in this study were 5A02 aluminum alloy and pure copper (T2), both with thickness of 3 mm. The chemical compositions of the base metals are listed in Tables 1 and 2, respectively. Both plates were machined into rectangle with 20 cm in length and 5 cm in width. The surfaces of both plates were cleaned by acetone prior to welding. After that, the plates were butt-welded together using load-controlled FSW equipment (FSW-3LM-003). The schematic of friction stir welding process and configuration of used tool is shown in Fig. 1. The rotating tool made of tool steel consisted of a flat edge concave shoulder with diameter of 12 mm and a conical pin with diameter of 3 mm.

The tool rotation speed, traverse speed and tool offset are main process parameters in determining the appearance and mechanical properties of FSWed joint. In the previous studies, various FSWed Al–Cu joints have already been obtained under different welding conditions. Therefore, the purpose of this study is not to optimize different process parameters. For obtaining defect-free joint, low welding speed and high rotation speed are usually required [32]. Based on previous studies and the literature review [33], the following process parameters were selected. Rotation speed and tool offset were kept constant, while the traverse speed was varied to obtain an acceptable joint with good weld appearance. After preliminary trials, the rotation rate was kept constant at 1100 rpm and the traverse speed was varied from 20 mm/min to 40 mm/min. During FSW, the tool tilted to the Al side of the weld and the tilt angle was kept 3° with respect to the vertical direction (i.e. Z-axis of FSW machine). The tool offset was 0.2 mm to the Al side, relative to the butt line. The plunge depth of rotational shoulder was 0.8 mm. The Cu was positioned on the retreating side (RS) and Al on the advancing side (AS), respectively.

After the FSW process, test specimens were sectioned transverse to the weldment. Standard metallographic preparation procedures were utilized. Macrostructures of the joints were examined by an optical microscope. Microstructure and fracture surface were observed using a scanning electron microscopy (SEM) equipped with an energy dispersive spectroscopy (EDS). The phase component at the WNZ was identified using a transmission electron microscopy (TEM). The focused ion beam (FIB) technique was used for preparing TEM foil of the bonded region. FIB-TEM specimen was prepared using an in situ lift out method. TEM with a Tecnai-G2 F30 operating at a nominal voltage of 300 kV was used to characterize the microstructure in detail. Phase identification was performed by selected-area electron diffraction (SAED). Images with a high atom number contrast (Z-contrast) were obtained using a high angle annular dark field (HAADF) detector in scanning transmission electron microscopy (STEM) mode. Vickers hardness measurement was performed at the top, middle and bottom portions of the cross-section with a load of 100 g for 10 s. Tensile tests were performed at room temperature using INSTRON 5569 testing machine at a crosshead speed of 1 mm/min, according to GB/T 2651-2008 standard (equivalent to ISO 9016: 2001) [34]. Three-point bending tests were conducted in accordance with the standard of GB/T 2653-2008 (equivalent to ISO 5173: 2000) [35].

Table 1
Chemical compositions of 5A02 aluminum alloy (wt.%).

Elements	Si	Fe	Cu	Mn	Mg	Ti	Al
5A02 aluminum alloy	0.40	0.40	0.10	0.15–0.40	2.0–2.8	0.15	Bal.

Table 2
Chemical compositions of copper (T2) (wt.%).

Elements	Cu + Ag	Fe	Bi	Sb	As	Pb	S
Copper	99.90	0.005	0.001	0.002	0.002	0.005	0.005

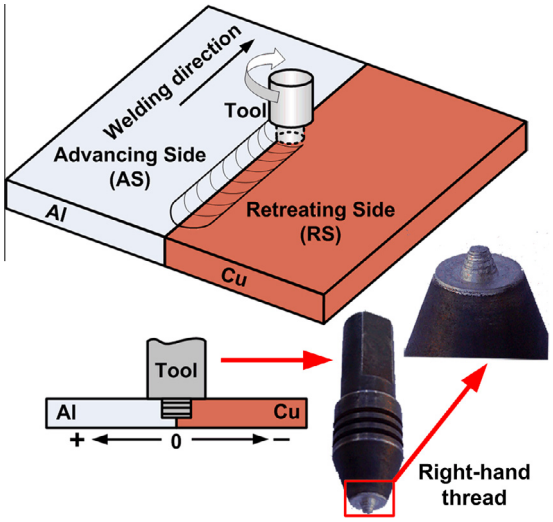

Fig. 1. Schematic of friction stir welding process and configuration of used tool.

3. Results and discussion

3.1. Joint appearance

Fig. 2 shows surface appearances and cross sections of Al/Cu joints produced at different traverse speeds. At traverse speed of 40 mm/min, the boundary of Al and Cu plates could be discernable from the surface appearance shown in Fig. 2a. Cavity defect was observed in the cross-sectional macrograph indicating incomplete mixing between Al and Cu. This defect was usually associated with insufficient material flow caused by insufficient heat input [36]. While at the lower welding speed of 20 mm/min, a good appearance with few flash was observed in Fig. 2c. The proper mixing occurred and void-free joint was obtained shown from cross section in Fig. 2d. The weld quality worsened instead with a further increase in traverse speed (Results not shown here). Unlike FSW of similar materials, typical cross section of FSW dissimilar joint was difficult to be divided into different regions such as thermo-mechanically affected zone (TMAZ), heat affected zone (HAZ) and weld nugget zone (WNZ). Moreover, the WNZ did not exhibit the classical onion ring structure due to different materials flow patterns [25,31]. According to the above results, a traverse speed of 20 mm/min was adopted thereafter as the optimal traverse speed for the welding experiments.

The weld quality was greatly influenced by the fixed location of tool pin besides process parameters (tool rotational speed, traverse speed and offset). Sound joints were obtained when hard plate, i.e., Cu was fixed at the retreating side (RS) under the welding conditions used in the present study. This finding was in consistent with the previous reports [36,37]. However, some researchers reported

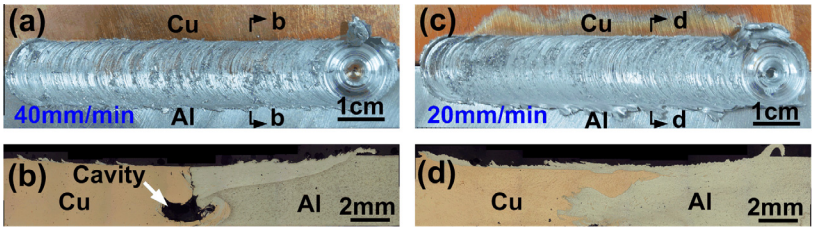

Fig. 2. Weld appearances and cross sections of friction stir welded joints at different traverse speeds: (a, b) 40 mm/min, (c, d) 20 mm/min.

that sound joints were achieved when Cu was fixed at the advancing side (AS) [25,31,32].

3.2. Microstructure and formation mechanism

Fig. 3 shows the microstructure of Al/Cu joint produced at traverse speed of 20 mm/min. All the micrographs were taken at the back-scattered electron (BSE) mode. Different phases were evidenced and corresponding EDS analysis were carried out. The EDS results were presented in Table 3. Fig. 3a shows an overview of SEM morphology at the stir zone of the Al/Cu joint. In the upper part of the weld, Cu bulk remained unbroken. The Al/Cu interface could be easily identified as shown in rectangle c. In comparison, violent stirring action was clearly observed in the lower part of the weld, indicated by rectangle d. The dispersion of the fine Cu fragments and particles was noticed at the nugget zone close to the Al matrix, as shown in Fig. 3b. These scattered fragments with irregular shapes and different sizes produced a composite-like structure. Similar phenomenon was observed by Xue et al. [24]. Inset of Fig. 3b shows the particles existed in the whole nugget zone. The nugget zone was thus strengthened by this kind of structure, which would be discussed later. High magnification of rectangle c shown in Fig. 3c indicated some structures (P1–P3) differing from base metals were generated close to Cu matrix. According to the EDS results of P1-P3, these structures were identified as Al_4Cu_9, Cu based Solid solution Cu (Al) and Al_2Cu, respectively. The newly formed isolated structures and solid solution may be related to the local diffusion induced by the mechanical effect of the tool pin. It could be seen from Fig. 3d that complex structure formed in the lower part of the weld, in which some different morphology could be distinguished. A large amount of finer and denser particles were dispersed in the Al matrix indicated in Fig 3e. Some Cu pieces

Table 3
EDS analysis results of reaction layer pointed in Fig. 3 (at.%).

Positions	Al	Cu	Possible phases
P1	27.47	72.53	Al_4Cu_9
P2	8.40	91.60	Solid solution Cu (Al)
P3	70.54	29.46	Al_2Cu
P4	67.64	32.36	Al_2Cu
P5	51.13	48.87	AlCu
P6	52.90	47.10	AlCu
P7	85.08	14.92	Al + Al_2Cu
P8	35.52	64.48	Al_2Cu_3
P9	68.09	31.91	Al_2Cu

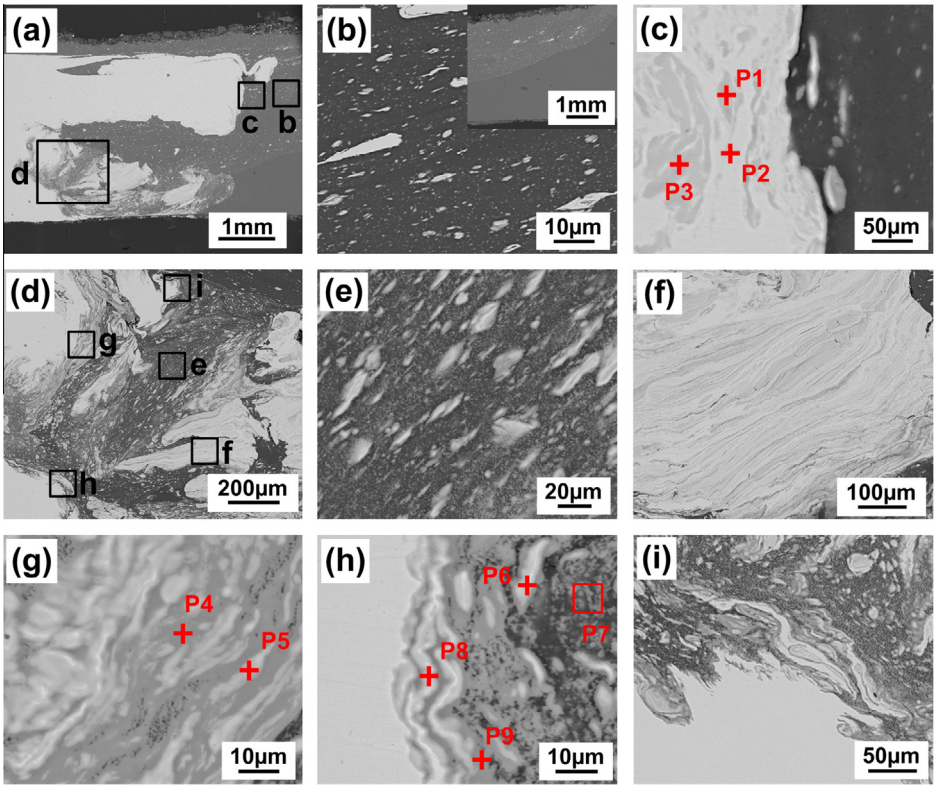

Fig. 3. Interfacial microstructure of Al/Cu joint produced at traverse speed of 20 mm/min: (a) overview of cross-section, (b–d) magnified views of regions b–d marked in (a), and (e–i) magnified views of regions e–i marked in (d).

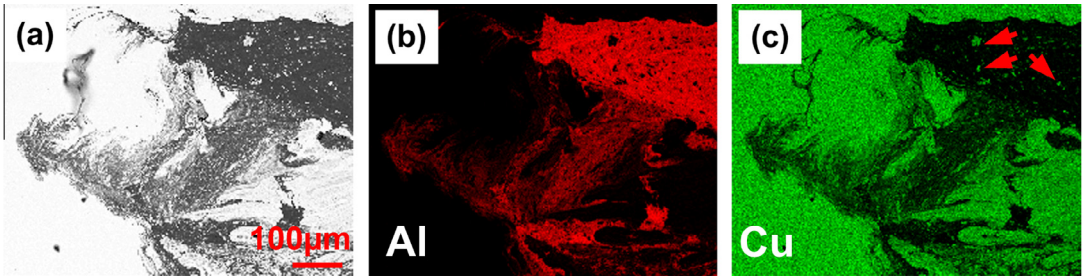

Fig. 4. EDS mapping of Al/Cu joint at the WNZ.

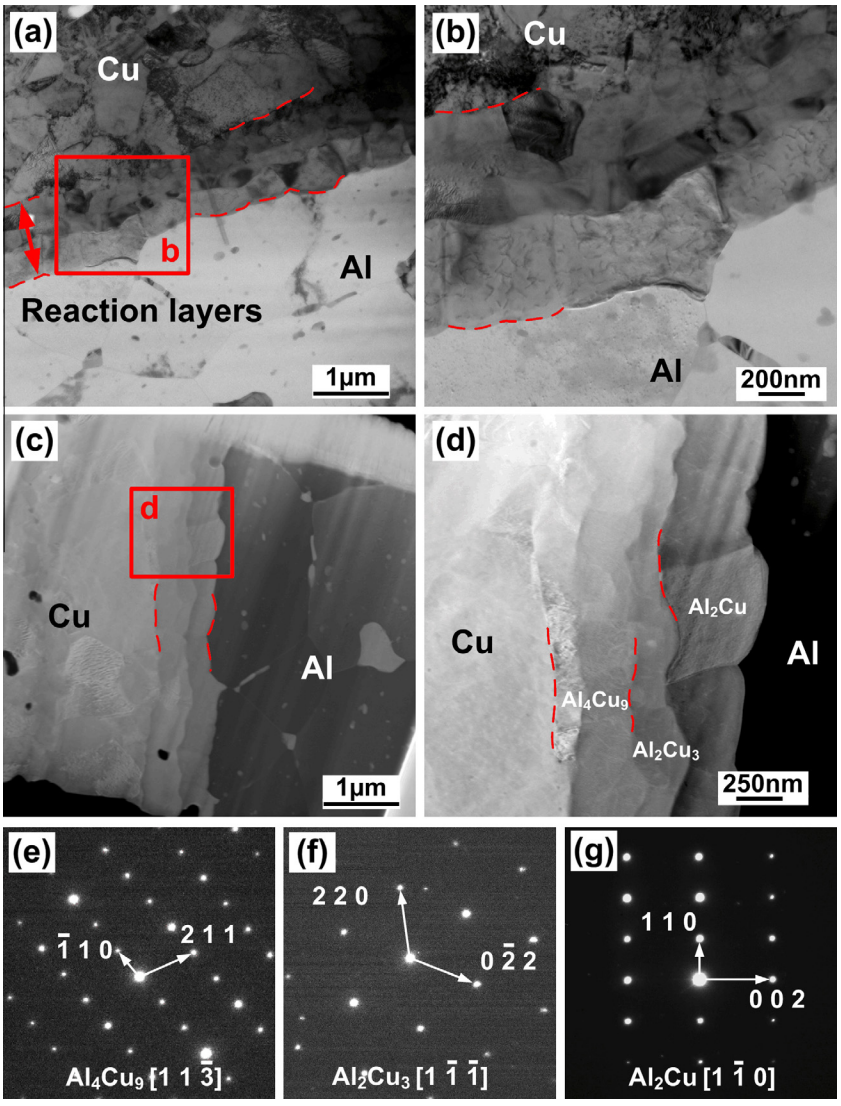

Fig. 5. TEM investigation of the Al/Cu interface: (a) bright field micrograph taken at the interface, (b) high magnification of (a), (c) HAADF micrographs corresponding to (a), (d) high magnification of (c), and (e–g) SAED patterns of interfacial reaction phases.

detached from the Cu bulk were stirred into the Al matrix giving rise to alternate lamella shown in Fig. 3f. The thickness of each lamella was not more than 30 μm. Besides, several different swirl and vortex-like patterns of layered structure could be evidenced, as shown from Fig. 3g to Fig. 3i. Based on the EDS analysis results, typical IMCs were observed in the lower part of the weld, including AlCu (P5 and P6), Al_2Cu_3 (P8) and Al_2Cu (P4, P7 and P9). Plastic stir action and friction heat generation were considered as the main reasons for the heterogeneous characteristics in the WNZ [22,24,31,36].

These swirl and vortex-like patterns have also been reported by Liu et al. [31]. But in some cases, only plastic deformation without any IMCs was observed in the Al/Cu joint [37]. This difference could be primarily associated with the heat input. With low heat input such as high traverse speed, the insufficient heat input could not induce interfacial reaction between Al and Cu. In contrast, the

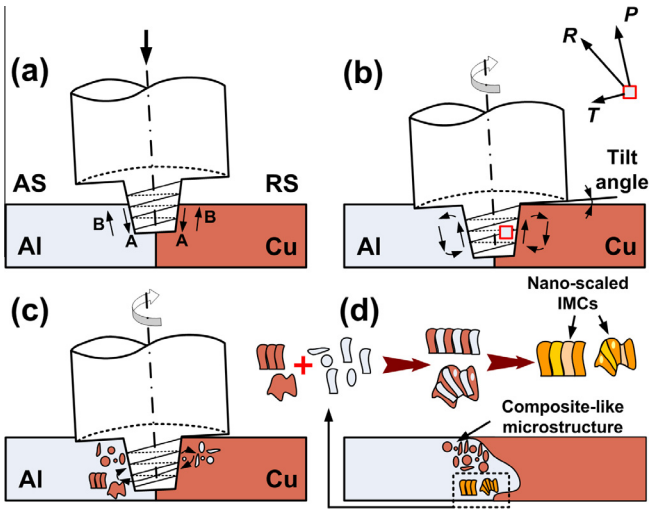

Fig. 6. Formation mechanism of composite-like structure and nano-scaled IMCs during FSW: (a) tool was plunged into workpiece, (b) material flowed when tool rotated, (c) fragments and particles were transported into each side and (d) formation of composite-like structure and nano-scaled microstructure.

IMCs were observed with the decreasing traverse speed in the aforementioned studies.

The element distribution of the WNZ is shown in Fig. 4. Good mixing of Al and Cu was noticed. According to the element distribution of Al and Cu, the bright particles in Fig. 4a mainly consisted of Cu element indicated by arrow in Fig. 4c. The refined Cu particles were involved into the Al matrix producing a composite-like structure, corresponding to the observation in Fig. 3. In addition, the slight variation of color contrast in Fig. 4b and c revealed the occurrence of interfacial reaction between Al and Cu due to the strong stirring action.

TEM analysis was performed to further identify the composition and structure of the reaction layers formed at the interface of Al/Cu. Fig. 5 shows TEM bright field (BF) micrographs and HAADF images with corresponding SAED patterns taken at the Al/Cu interface. As shown in Fig. 5a, an ultra-thin and continuous layer with thickness of approximately 1 μm was clearly observed from the BF image. The fine grains were visible at higher magnification in Fig. 5b. It was difficult to distinguish the reaction phases in BF mode. *Z*-contrast images of these newly formed reaction phases were thus observed, as shown in Fig. 5c. For the HAADF STEM micrograph, higher magnification in Fig. 5d showed three different nano-scaled reaction layers. Based on the SAED pattern calibration result, the reaction layers from Cu side to Al side were indexed as Al_4Cu_9 (γ), Al_2Cu_3 (ε), Al_2Cu (θ), respectively. Al_4Cu_9 (γ) and Al_2Cu (θ) were two most common phases reported in previous studies [10,21–24,31,32]. However, limited literature mentioned the formation of Al_2Cu_3. Xia et al. [11] reported this phase formed at the interface when vacuum brazing of Al and Cu using Al–Si filler metal. Another phase AlCu (η) detected in SEM was not found in the TEM specimen since the range of observation was restricted to a very small region. It was worth noticing that these nano-scaled structures were not observed in the case of higher traverse speed.

Based on the microstructural analysis above, the formation mechanism was expected to be elucidated with the assistance of Fig. 6. First, when the pin was plunged into the workpiece, the metal adjacent to the threaded pin flowed downward due to the external pressure (arrow A) while the surrounding metal was extruded upwards (arrow B) as shown in Fig. 6a [38]. The metal flowing upward was extruded downward when the pin was completely inserted into the workpiece and the shoulder was in direct contact with the surface of the deformed metals. When the tool traversed along the joint line, the material flow was closely associated with the pin thread orientation and tool rotational direction [39]. Two forces was applied to the plasticized material around the pin. One was pressure *P* acting in the direction perpendicular to the thread surface because of the rotation of the pin tool, the other was traction force *T* which was parallel to the thread surface resulting from the friction between the thread surface and the plasticized material [40]. In this case (right-hand thread), under the combined action of those two forces, the plasticized material was transported upward from the bottom of the RS following a direction of resultant force *R*, indicated in Fig. 6b. Cu detached from bulk was thus cracked into smaller fragments with different sizes. The metals were then deposited at the trailing side of the pin tool (Fig. 6c). As the tool rotated, Al and Cu were transported into each side. Al and Cu bulk were thus trapped and kneaded acting like an extrusion die. The Temperature of the local weld rose rapidly at the combined action of frictional heat and plastic deformation. In such a case, the Al and Cu atoms were activated inducing interdiffusion at the interface [32]. The smaller Cu particles were dispersed into the Al matrix giving rise to the composite-like structure. Some large fragments subsequently reacted with Al pieces and matrix producing layered structure and intercalation structure, as shown

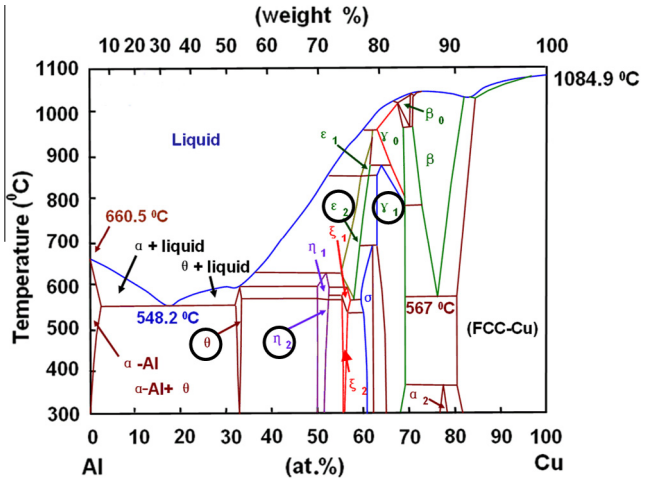

Fig. 7. Binary diagram of Al–Cu.

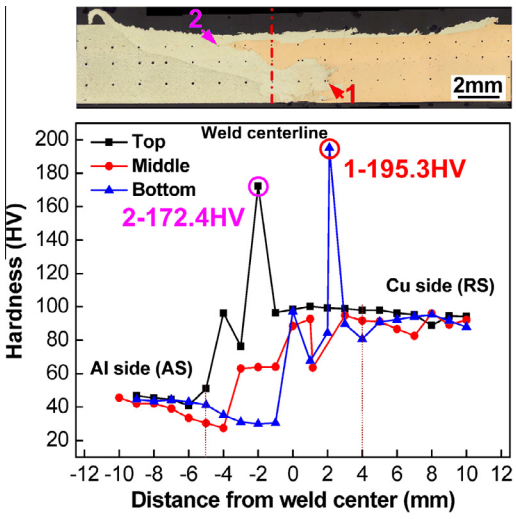

Fig. 8. Hardness profiles along top, middle and bottom lines of transverse cross-section.

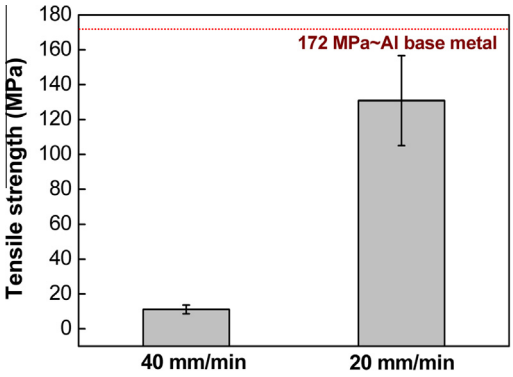

Fig. 9. Tensile shear strength of FSWed Al/Cu joints.

in Fig. 6d. According to the ratio of elements Al and Cu, the nano-scaled stoichiometric IMCs Al_4Cu_9 (γ), Al_2Cu_3 (ε) and Al_2Cu (θ) formed along the direction moving from Cu side to Al side. In some occasion, the phase AlCu (η) formed as well. The formation mechanism of newly formed structure in FSW was quite different from that in fusion welding, which could be seen from Al–Cu binary diagram [41] shown in Fig. 7. Temperature history measured by Liu et al. [31] suggested that the peak temperature the weld experienced was much lower than the melting point of Al and Cu. In other words, the interfacial reaction of Al and Cu was realized during FSW with heat input far lower than that needed in fusion welding. Therefore, the thickness of IMCs could be controlled to nano scale while achieving metallurgical bonding. This composite-like structure and nano-scaled layered structure would have significant influence on mechanical properties of the Al/Cu dissimilar joint.

3.3. Mechanical properties

3.3.1. Microhardness distribution

The micro Vickers hardness distribution profile on the transverse cross-section of the joint welded at traverse speed of 20 mm/min is shown in Fig. 8. The average hardness values of base metals Al and Cu were 46 HV and 94 HV, respectively. The hardness of HAZ in Al side was lower than that of base metal due to HAZ softening. The occurrence could be probably attributed to the grain coarsening and dissolution of strengthening precipitates induced by the thermal cycle of the FSW process [42]. An inhomogeneous distribution of hardness values was observed in the WNZ. The higher hardness value in the WNZ relative to Al base metal was primarily associated with the formation of very fine recrystallized grains and the Cu-rich dispersed particles, corresponding to the observation in Fig. 3b. It is worth noticing that an abrupt change in hardness value occurred adjacent to the interface. The values at the interface of top and bottom reached 172.4 HV and 195.3 HV, which were far higher than that of Al and Cu base metals. The distinct rise in hardness at the interface was attributed to the presence of nano-scaled IMCs, which was in good consistent with the observation in Fig. 5.

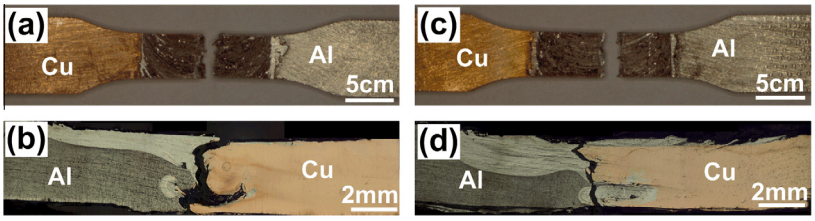

Fig. 10. Fracture locations at different traverse speeds corresponding to Fig. 9: (a, b) 40 mm/min; (c,d) 20 mm/min.

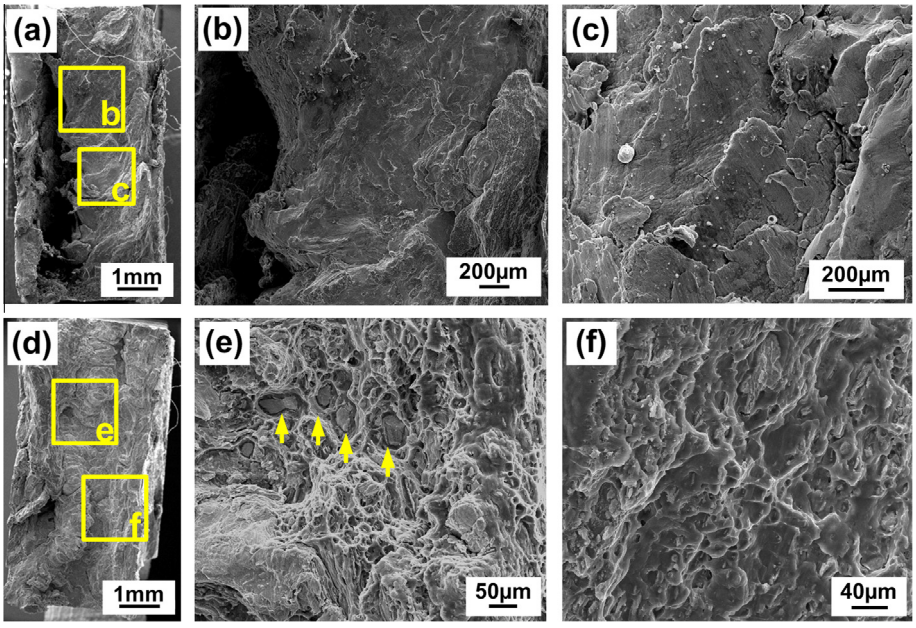

Fig. 11. Fracture surface morphologies of joints produced at 40 mm/min (a–c) and 20 mm/min (d–f): (a and d) overview of fracture surface; (b, c) high magnification of regions b and c marked in (a); (e, f) high magnification of regions e and f marked in (d).

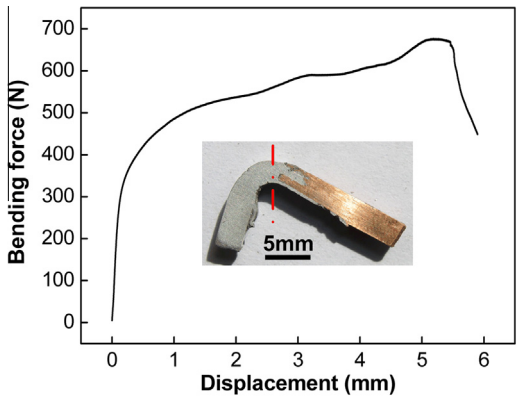

Fig. 12. Bending strength of Al/Cu joint produced at traverse speed of 20 mm/min.

3.3.2. Tensile strength and fracture behavior

Fig. 9 shows the tensile strength of joints welded at different traverse speed corresponding to Fig. 2. The tensile strength of joint produced at relatively fast traverse speed of 40 mm/min was rather weak with average value of 11 MPa. However, the average strength of joint fabricated at traverse speed of 20 mm/min reached 130 MPa, representing joint efficiency of 75.6% of the Al alloy base metal.

Fig. 10 shows fracture locations in both cases indicated in Fig. 9. Some differences could be distinguished from their fracture locations, although both joints fractured at the stir zones as shown in Fig. 10a and c. For joint welded at traverse speed of 40 mm/min, the voids acted as fracture initiation sites during tensile testing shown in Fig. 10b. The crack initiated from the cavity defect and propagated to the joining zones in the upper part of the plate. In the case of joint produced at 20 mm/min, the zigzag feature was observed. From Fig. 9d, the crack propagation was found along the Al/Cu border in the upper weld but extended into the stir zone close to Al side in the lower part. This fracture behavior showed the reaction phases at the lower weld exhibited high resistance to crack propagation.

Fig. 11 shows the SEM morphologies of fracture surfaces corresponding to Fig. 10. It could be observed from Fig. 11a that the feature of fracture surface was characterized by smooth surface without severe deformation indicated in Fig. 11b and c. The cavity defect coupled with no metallurgical bonding resulted in the low strength shown in Fig. 9. However, in Fig. 11e and f the fracture morphology of joint with lower traverse speed was characterized by dimples in different sizes. Dispersed Cu particles were observed in the dimples indicating the occurrence of tearing in the stir zone. Compared with Fig. 11c, Fig. 11f showed the larger dimples indicating these strengthening particles played a significant role in preventing crack propagation.

3.3.3. Bending strength

Bending properties was tested to determine the ductility of the defect-free Al/Cu joints which are always required in electric power industry. Fig. 12 shows the bending load versus displacement as well as the appearance of the sample after the bending test. The bending load was applied in the weld center viewed from the back surface. No crack was observed on the outer surface after the bending test, indicating the joint had a good ductility.

In sum, bonding strength of Al–Cu joint was greatly enhanced by two strengthening mechanisms. The WNZ was reinforced by the dispersion of fine Cu-rich particles in the Al matrix. Excellent metallurgical bonding of the Al–Cu interface was improved by formation of the nano-scaled, continuous and uniform IMCs layers. As a result, good mechanical behaviors were achieved.

4. Conclusions

In this study, the microstructure of FSWed Al/Cu joint and its formation mechanism were identified and discussed. In addition, the relationship between microstructure and mechanical properties was investigated. The following conclusions were made:

(1) 5A02 aluminum alloy and pure copper were successfully joined by FSW under the condition of rotation speed 1100 rpm, traverse speed 20 mm/min, the tool offset 0.2 mm relative to the weld centerline and Al sheet at the advancing side. High rotation speed and low traverse speed were required. If not, the cavity defect was easily produced.
(2) Heterogeneous structure was observed in the WNZ. Cu detached from bulk was cracked into fine particles. In the upper part of the WNZ, the dispersion of these particles and fragments in the Al matrix produced a composite-like structure. In the lower part, the intercalation and swirl-like pattern were evidenced due to strong stir action.
(3) Thin, continuous and uniform layers were observed at the Al/Cu interface, which were identified by TEM–HAADF analysis. Nanoscaled phase Al_4Cu_9 (γ), Al_2Cu_3 (ε), Al_2Cu (θ) were characterized, respectively. The presence of IMCs gave rise to the distinct rise in hardness at the Al/Cu interface.
(4) Composite-like structure and nano-scaled reaction layers caused an excellent metallurgical bonding and increased mechanical strength. Tensile strength could reach 130 MPa, representing joint efficiency of 75.6% of the Al alloy base metal. No crack was observed on the appearance after the bending test.

Acknowledgements

One of the authors (C.W. Tan) is grateful for the financial support by the China Scholarship Council for one year study at University of Waterloo, Canada. The assistance of Dr. Y.X. Huang and Dr. D.Z. Chi in performing the experiments is gratefully acknowledged. We also express our gratitude to Professor Y. Zhou at University of Waterloo, Canada, for his helpful discussion.

References

[1] Fazel-Najafabadi M, Kashani-Bozorg SF, Zarei-Hanzaki A. Dissimilar lap joining of 304 stainless steel to CP-Ti employing friction stir welding. Mater Des 2011;32:1824–32.
[2] Simoncini M, Forcellese A. Effect of the welding parameters and tool configuration on micro- and macro-mechanical properties of similar and dissimilar FSWed joints in AA5754 and AZ31 thin sheets. Mater Des 2012;41:50–60.
[3] Bang HS, Bang HS, Jeon GH, Oh IH, Ro CS. Gas tungsten arc welding assisted hybrid friction stir welding of dissimilar materials Al6061-T6 aluminum alloy and STS 304 stainless steel. Mater Des 2012;37:48–55.
[4] Ji F, Xue S, Dai W. Reliability studies of Cu/Al joints brazed with Zn–Al–Ce filler metals. Mater Des 2012;42:156–63.
[5] Honarpisheh M, Asemabadi M, Sedighi M. Investigation of annealing treatment on the interfacial properties of explosive-welded Al/Cu/Al multilayer. Mater Des 2012;37:122–7.
[6] Sedighi M, Honarpisheh M. Experimental study of through-depth residual stress in explosive welded Al–Cu–Al multilayer. Mater Des 2012;37:577–81.
[7] Mai TA, Spowage AC. Characterisation of dissimilar joints in laser welding of steel–kovar, copper–steel and copper–aluminum. Mater Sci Eng A 2004;374:224–33.
[8] Mozhaiskaya TM, Chekanova NT. Structure and properties of welded aluminum–copper joints. Met Sci Heat Treat 1990;32(12):938–9.
[9] Abbasi M, Karimi Taheri A, Salehi MT. Growth rate of intermetallic compounds in Al/Cu bimetal produced by cold roll welding process. J Alloy Compd 2001;319:233–41.
[10] Sheng LY, Yang F, Xi TF, Lai C, Ye HQ. Influence of heat treatment on interface of Cu/Al bimetal composite fabricated by cold rolling. Composites: Part B 2011;42:1468–73.

[11] Xia C, Li Y, Puchkov UA, Gerasimov SA, Wang J. Microstructure and phase constitution near the interface of Cu/Al vacuum brazing using Al–Si filler metal. Vacuum 2008;82:799–804.
[12] Eslami P, Taheri AK. An investigation on diffusion bonding of aluminum to copper using equal channel angular extrusion process. Mater Lett 2011;65:1862–4.
[13] Asemabadi M, Sedighi M, Honarpisheh M. Investigation of cold rolling influence on the mechanical properties of explosive-welded Al/Cu bimetal. Mater Sci Eng A 2012;558:144–9.
[14] Chen SY, Wu ZW, Liu KX, Li XJ, Luo N, Lu GX. Atomic diffusion behavior in Cu–Al explosive welding process. J Appl Phys 2013;113(4):044901–44906.
[15] Lee WB, Bang KS, Jung SB. Effects of intermetallic compound on the electrical and mechanical properties of friction welded Cu/Al bimetallic joints during annealing. J Alloy Compd 2005;390:212–9.
[16] Sahin M. Joining of aluminum and copper materials with friction welding. Int J Adv Manuf Technol 2010;49:527–34.
[17] Wanjara P, Dalgaard E, Trigo G, Mandache C, Comeau G, Jonas JJ. Linear friction welding of Al–Cu: Part 1-Process evaluation. Can Metall Quart 2011;50(4):350–9.
[18] Dalgaard E, Wanjara P, Trigo G, Jahazi M, Comeau G, Jonas JJ. Linear friction welding of Al–Cu: Part 2-Interfacial characteristics. Can Metall Quart 2011;50(4):360–70.
[19] Thomas WM, Nicholas ED, Needham JC, Murch MG, Templesmith P, Dawes CJ. GB Patent Application No. 9125978.8; 1991.
[20] Murr LE, Li Y, Flores RD, Trillo EA, McClure JC. Intercalation vortices and related microstructural features in the friction-stir welding of dissimilar metal. Mater Res Innov 1998;2(3):150–63.
[21] Ouyang JH, Yarrapareddy E, Kovacevic R. Microstructural evolution in the friction stir welded 6061 aluminum alloy (T6-temper condition) to copper. J Mater Process Technol 2006;172:110–22.
[22] Abdollah-zadeh A, Saeid T, Sazgari B. Microstructural and mechanical properties of friction stir welded aluminum/copper lap joints. J Alloy Compd 2008;460:535–8.
[23] Saeid T, Abdollah-zadeh A, Sazgari B. Weldability and mechanical properties of dissimilar aluminum–copper lap joints made by friction stir welding. J Alloy Compd 2010;490:652–5.
[24] Xue P, Xiao BL, Ni DR, Ma ZY. Enhanced mechanical properties of friction stir welded dissimilar Al–Cu joint by intermetallic compounds. Mater Sci Eng A 2010;527:5723–7.
[25] Xue P, Ni DR, Wang D, Xiao BL, Ma ZY. Effect of friction stir welding parameters on the microstructure and mechanical properties of the dissimilar Al–Cu joints. Mater Sci Eng A 2011;528:4683–9.
[26] Galvão I, Leal RM, Loureiro A, Rodrigues DM. Material flow in heterogeneous friction stir welding of aluminum and copper thin sheets. Sci Technol Weld Joining 2010;15:654–60.
[27] Galvão I, Oliveira JC, Loureiro A, Rodrigues DM. Formation and distribution of brittle structures in friction stir welding of aluminum and copper: influence of process parameters. Sci Technol Weld Joining 2011;16(8):681–9.
[28] Galvão I, Oliveira JC, Loureiro A, Rodrigues DM. Formation and distribution of brittle structures in friction stir welding of aluminum and copper: Influence of shoulder geometry. Intermetallics 2012;22:122–8.
[29] Galvão I, Loureiro A, Verdera D, Gesto D, Rodrigues DM. Influence of tool offsetting on the structure and morphology of dissimilar aluminum to copper friction-stir welds. Metall Mater Trans A 2012;43:5096–105.
[30] Galvão I, Leitão C, Loureiro A, Rodrigues DM. Study of the welding conditions during similar and dissimilar aluminum and copper welding based on torque sensitivity analysis. Mater Des 2012;42:259–64.
[31] Liu HJ, Shen JJ, Zhou L, Zhao YQ, Liu C, Kuang LY. Microstructural characterisation and mechanical properties of friction stir welded joints of aluminum alloy to copper. Sci Technol Weld Joining 2011;16(1):92–9.
[32] Genevois C, Girard M, Huneau B, Sauvage X, Racineux G. Interfacial reaction during friction stir welding of Al and Cu. Metall Mater Trans A 2011;42(8):2290–5.
[33] Bisadi H, Tavakoli A, Sangsaraki MT, Sangsaraki KT. The influences of rotational and welding speeds on microstructures and mechanical properties of friction stir welded Al5083 and commercially pure copper sheets lap joints. Mater Des 2013;43:80–8.
[34] GB/T 2650-2008/ISO 6-9016:2001. Tensile test method on welded joints. Standardization Administration of the People's Republic of China; 2008.
[35] GB/T 2653-2008/ISO 5173:2000. Bend test methods on welded joints. Standardization Administration of the People's Republic of China; 2008.
[36] Firouzdor V, Kou S. Al–Cu friction stir lap welding. Metall Mater Trans A 2012;43(1):303–15.
[37] Liu P, Shi QY, Wang W, Wang X, Zhang ZL. Microstructure and XRD analysis of FSW joints for copper T2/aluminum 5A06 dissimilar materials. Mater Lett 2008;62:4106–8.
[38] Cui GR, Ma ZY, Li SX. Peroidical plastic flow pattern in friction stir processed Al–Mg alloy. Scripta Mater 2008;58:1082–5.
[39] Xu WF, Liu JH, Chen DL. Material flow and core/multi-shell structures in a friction stir welded aluminum alloy with embedded copper markers. J Alloy Compd 2011;509:8449–54.
[40] Chowdhury SM, Chen DL, Bhole SD, Cao X. Tensile properties of a friction stir welded magnesium alloy: Effect of pin tool thread orientation and weld pitch. Mater Sci Eng A 2010;527:6064–75.
[41] ASM Handbooks. Alloy phase diagrams, Vol. 3. Materials Park (OH): ASM International; 2002.
[42] Singh RKR, Sharma C, Dwivedi DK, Mehta NK, Kumar P. The microstructure and mechanical properties of friction stir welded Al–Zn–Mg alloy in as welded and heat treated conditions. Mater Des 2011;32:682–7.